

Article

Towards Intense THz Spectroscopy on Water: Characterization of Optical Rectification by GaP, OH1, and DSTMS at OPA Wavelengths

Fabio Novelli ^{1,*},[†] , Biswajit Guchhait ^{1,2,†} and Martina Havenith ^{1,*}

¹ Department of Physical Chemistry II, Ruhr University Bochum, 44801 Bochum, Germany; biswajit.guchhait@snu.edu.in

² Department of Chemistry, School of Natural Sciences, Shiv Nadar University, Greater Noida, Uttar Pradesh 201314, India

* Correspondence: fabio.novelli@ruhr-uni-bochum.de (F.N.); martina.havenith@rub.de (M.H.)

† Contributed equally.

Received: 11 February 2020; Accepted: 10 March 2020; Published: 13 March 2020



Abstract: Water is the most prominent solvent. The unique properties of water are rooted in the dynamical hydrogen-bonded network. While TeraHertz (THz) radiation can probe directly the collective molecular network, several open issues remain about the interpretation of these highly anharmonic, coupled bands. In order to address this problem, we need intense THz radiation able to drive the liquid into the nonlinear response regime. Firstly, in this study, we summarize the available brilliant THz sources and compare their emission properties. Secondly, we characterize the THz emission by Gallium Phosphide (GaP), 2-(3-(4-hydroxystyryl)-5,5-dimethylcyclohex-2-enylidene)malononitrile (OH1), and 4-N,N-dimethylamino-4'-N'-methyl-stilbazolium 2,4,6-trimethylbenzenesulfonate (DSTMS) crystals pumped by an amplified near-infrared (NIR) laser with tunable wavelength. We found that both OH1 as well as DSTMS could convert NIR laser radiation between 1200 and 2500 nm into THz radiation with high efficiency ($> 2 \times 10^{-4}$), resulting in THz peak fields exceeding 0.1 MV/cm for modest pump excitation (\sim mJ/cm²). DSTMS emits the broadest spectrum, covering the entire bandwidth of our detector from ca. 0.5 to \sim 7 THz, also at a laser wavelength of 2100 nm. Future improvements will require handling the photothermal damage of these delicate organic crystals, and increasing the THz frequency.

Keywords: terahertz; water; solvation; hydration; non-linear optics; spectroscopy

1. Introduction

Terahertz (THz) radiation probes the collective intermolecular modes of hydrogen-bonded water molecules from \sim 0.2 to \sim 20 THz [1]. These modes [1–5] represent the microscopic solvent coordinate for proton transfer [6], are involved in bio-reactions like drug intercalation into DNA [7,8] and, according to molecular dynamics simulations [9], are the drive of the structural rearrangements of the molecular network. The collective transient dynamics of the hydrogen-bonded network dictate the unique solvation properties of water, and are at the origin of the puzzling physical and chemical properties of this special liquid [10–12]. However, pivotal issues remain about the interpretation of these THz features [13]. For example, mapping how the energy dissipates upon excitation of a low frequency mode could allow a deeper understanding and, possibly, engineering of solvation processes [14,15].

While infrared spectroscopy (IR) typically probes intramolecular modes, the absorption features in the THz range can be broad [16]. These broad bands reveal properties related to the hydration of small or large solutes, including proteins [17]. Previous molecular dynamics (MD) calculations [1] indicated that

different excitations are present in the IR (>30 THz) and THz ranges (<30 THz). While the intramolecular modes in the IR involve strong electronic couplings, the THz bands are linked to correlated intermolecular motions. MD also found that the water absorption band centered at ~6 THz can be described by dynamics extending to the first solvation shell. Below 3 THz, the collective nature and delocalized character of these low-frequency modes dominates, which involve systematic correlations of particle motion beyond the first solvation shell. Below 0.2 THz, the dielectric response of water is dominated by a band centered at ~20 GHz [18]. This band can be fitted to a Debye relaxation with a reorientation time of ~8 ps. While the original Debye model holds for non-interacting molecules exposed to an external electric field, the precise description of this band implies nontrivial microscopic mechanisms in the hydrogen-bonded network. Understanding this dielectric response of water is still a challenge above 20 GHz, up to the THz range [19–22]. The Debye-like reorientation mode is sketched on the left in Figure 1a.

At equilibrium, the absorption by liquid water in the THz spectrum is continuous and characterized by two prominent bands [23] that have been assigned to the hindered translational (centered at ~6 THz) and rotational (from ca. 10 to 20 THz) modes of the hydrogen-bonded water molecules [1,16]. The THz spectrum of pure liquid water at $T = 20\text{ }^{\circ}\text{C}$ is shown in Figure 1. In order to fit the band centered at ~20 THz shown in Figure 1b, at least two hindered rotational (or librational) modes are needed [24–26]. The infrared active rotations of a single water molecule have been assigned to the “rocking” and the “wagging”, while the “twisting” should be exclusively active in Raman experiments [26]. For this reason, and based on the different rotational constants, it is possible to tentatively assign the band centered at ~15 THz to the rocking librations of H-bonded waters. The band at ~21 THz can be associated to wagging librations. Cartoons of THz modes are sketched in Figure 1a.

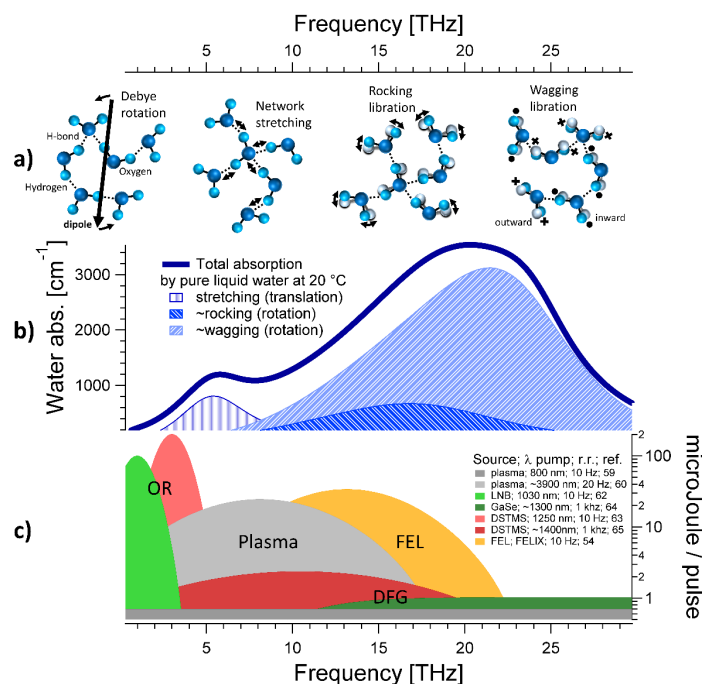


Figure 1. (a) Cartoons of the different modes of liquid water in the TetraHertz (THz) range. Below 1 THz, the dielectric response is dominated by the Debye-like reorientation of the collective dipole of H-bonded water molecules [18–22]. Intermolecular translations or “network stretching” modes are centered at ca. 6 THz, while librational modes are found between ~10 and ~20 THz [24–26]. (b) Equilibrium absorption coefficient of pure water at $T = 20\text{ }^{\circ}\text{C}$ [1–4]. A minimal fit reveals at least three bands that can be associated to the intermolecular modes sketched in panel (a). (c) Summary of the most intense THz sources reported to date. Gray: plasma generation; green: emission from inorganic crystals by non-linear optical methods; red: emission from organic materials; orange: frequency region of a pump-probe experiment operating at a free electron laser. The laser wavelength, repetition rate (r.r.), and the reference number is indicated. See text for further details.

In order to explore the complex energy landscape of liquid water and address its unique solvation properties, highly brilliant THz sources are required. Unfortunately, it is challenging to generate intense radiation in the so-called “THz gap”, which nowadays spans between about 7 and 19 THz and largely overlaps with water librations. We report in Figure 1c, to the best of our knowledge, the few available sources delivering pulsed radiation exceeding one $\mu\text{J}/\text{pulse}$ in the THz range.

There are two ways to generate intense THz pulses [27]. The first exploits current effects, i.e., the fact that a time-varying charge current can act as a radiation source [27]. This basic concept holds for antennas [28–33], which are widely used in conjunction with non-amplified pulsed lasers to perform terahertz time-domain spectroscopy, and for particle accelerators, where relativistic electron beams are deflected by magnets and thereby emit radiation of tunable wavelength [34–36] that can cover the THz range [37–52]. While accelerators can cover a large frequency range, these complex machines are often optimized for a certain range because optical elements have limited bandwidths [53]. For example, as sketched in orange in Figure 1c, single color pump-probe experiments at the free electron laser (FEL) facility FELIX in Nijmegen can currently be performed only between ca. 5 and 25 THz [54]. The severe beam time restrictions at the few available facilities, and the limited tunability in polarization and pulse length constrain the applicability of these sources.

Furthermore, THz generation is reported on using novel spintronic devices [55,56] as well as the broadband THz emission by plasma filaments [57,58]. Typically, THz emission by filaments is triggered by focusing into air the first and second harmonics of a fundamental near-infrared (NIR) amplified laser [57,58]. Dey et al. [59] demonstrated enhanced broadband intense THz generation by filamentation in liquids, with about 1 $\mu\text{J}/\text{pulse}/\text{THz}$ and spanning from ~ 0.1 to 50 THz (see the dark gray plot in Figure 1c. Recently, Koulouklidis et al. [60] proposed an extremely brilliant THz source by two color filamentation of MIR laser pulses with the fundamental wavelength set to 3.9 μm . Conversion efficiency above 2% and electric fields of more than 100 MV/cm were demonstrated spanning between ca. 3 and 11 THz. We sketch the corresponding spectrum with the light gray curve in Figure 1c.

Another way to generate THz is based on non-linear optical methods, by which a strong laser (often in the NIR) induces a non-linear polarization in a birefringent medium. In turn, the non-linear polarization can be the source of pulsed radiation [61]. Emission in the THz range can be achieved through optical rectification (OR) [62,63], by which the wavelength bandwidth of an infrared laser pulse is converted into an intrinsically phase-stable THz field, or by the difference frequency (DFG) [64,65] of two NIR pulses oscillating at slightly different frequencies. OR typically allows us to generate intense THz radiation below 5 THz (sketched in light green and light red in Figure 1c), while DFG covers higher frequencies (dark green and dark red in Figure 1c). Both inorganic (LiNbO₃ [66–77], GaSe [78–80], ZnTe [81,82], LiGaS₂ [83], GaP [84–89]) as well as organic (DSTMS [89–92], OH1 [93–97], DAST [98,99], DPFO [100], HMQ-TMS [101], OHQ-N2S [102]) crystals are phase-matched in the NIR and can emit pulsed THz fields with peak amplitudes in excess of 1 MV/cm. The approximate spectrum of the strongest THz pulses generated to date by non-linear optical methods in inorganic [62,64] and organic [63,65] crystals are shown in green and in red in Figure 1c, respectively.

The detection of THz radiation is based on similar concepts. The highest dynamic range (DR) reported to date is above 100 dbm when antennas are used in conjunction with multi-MHz laser oscillators [103,104]. For amplified NIR sources operating in the kHz range, we recently demonstrated [29] a fast scan acquisition technique based on the Pockels effect [37] with a DR of more than 60 dbm. Both techniques operate in a limited frequency range and can detect THz radiation up to ~ 7 THz. Broader THz spectra can be measured with thin crystals [89,105], via more exotic detection schemes employing organic crystals with large linear birefringence [106–110], or with air-biased coherent detection (ABCD) at a cost of reduced DR (~ 30 dbm) [111–113]. While the detection techniques described above allow measuring both the amplitude as well as the phase of a THz field, power or intensity detectors are also available over the entire THz range [114,115].

In the quest to find intense sources operating in the THz gap, here, we report the experimental characterization of the OR in GaP, OH1, and DSTMS over the full range of the wavelengths emitted by an optical parametric amplifier (OPA), i.e., between 1200 and 2500 nm.

2. Materials and Methods

An amplified Ti:Sa laser (Astrella, Coherent, Santa Clara, CA, USA) emits 90 fs long pulses centered at 790 nm with a repetition rate of 1 kHz. Part of the fundamental laser output (ca 2 mJ/pulse) seeds a commercial and automated OPA (TOPAS TWINS, Light Conversion). The non-linear process of parametric amplification generates simultaneously both the signal (s) as well as the idler (i) beams [61]. The total output power of the OPA (s+i) is between 0.6 and 0.8 W for the investigated wavelengths. We separate the s and i beams with a polarizing beam-splitter provided by the manufacturer. We use only one “pump” beam at a time, either s or i, to generate THz radiation. The selected pump pulse is focused down to a ~1 mm full width half maximum (FWHM) spot size into the crystal used to generate THz. We chop the pump beam at 500 Hz and adjust the pump fluence with neutral density filters. We keep the pump fluence well below the damage threshold, and set it to obtain peak THz fields of approximately 100 kV/cm.

Here we investigate the THz emission by ~0.5 mm thick crystals (GaP, DSTMS, and OH1) triggered by pump pulses centered at $\lambda_P = 1200$ (s), 1400 (s), 1600 (s), 2100 (i), 2300 (i), 2500 nm (i). We chose the wavelengths to avoid photodamage. OH1 [116] (DSTMS [117,118]) strongly absorbs at 1500, 1800, and 2000 nm (1700 and 1800 nm). We recorded the generated THz fields by electro-optical sampling [32,37,81,119–121] in another 0.5 mm thick GaP crystal. The emitted field is probed by a 790 nm laser beam detected by balanced photo diodes (PDB210A, Thorlabs, Newton, NJ, USA) and lock-in amplification with a boxcar averager (UHFLI, Zurich Instruments, Zurich, Switzerland). The photovoltage is converted into field amplitude (kV/cm) by considering the electro-optical coefficient, index of refraction, and thickness of the detection crystal (see e.g., Equation (17) in [37]). We enclose the setup into a plastic box and purge with nitrogen to reduce the water vapor content to below 10%.

3. Results

In the following, we report the THz emission by both the inorganic GaP as well as the organic DSTMS and OH1 crystals (Rainbow Photonics, Zurich, Switzerland) at the OPA wavelengths. The results are summarized in Figures 2–4, displaying the THz emission by ~0.5 mm thick GaP, OH1 and DSTMS, respectively.

3.1. Gallium Phosphide (GaP)

Figure 2a displays the THz fields generated for different pump wavelengths, all obtained at the same pump fluence of 19.1 mJ/cm². The transient THz pulses are detected by delaying the arrival time of the electro-optical sampling beam (t_{EOS}). We obtain almost single-cycle fields with a duration of ca. 0.35 ps (time difference between the minimum at $t_{EOS} \sim -0.15$ ps and the next minimum at $t_{EOS} \sim +0.2$ ps). This duration increases for longer pump wavelengths. A THz peak field of ~30 kV/cm is obtained at $t_{EOS} = 0$ ps and for $\lambda_P = 1200, 1400,$ and 1600 nm. The THz field amplitude emitted by the non-linear optical process of OR should scale linearly with the intensity of the driving pump field [61], which is confirmed in Figure 2b. We chose the intermediate pump wavelength of $\lambda_P = 1600$ nm and varied the fluence from 3.2 mJ/cm² to 19.1 mJ/cm². We found a linear relationship between the THz field and the pump intensity, as indicated by the black line fit with an R^2 value of 1.02.

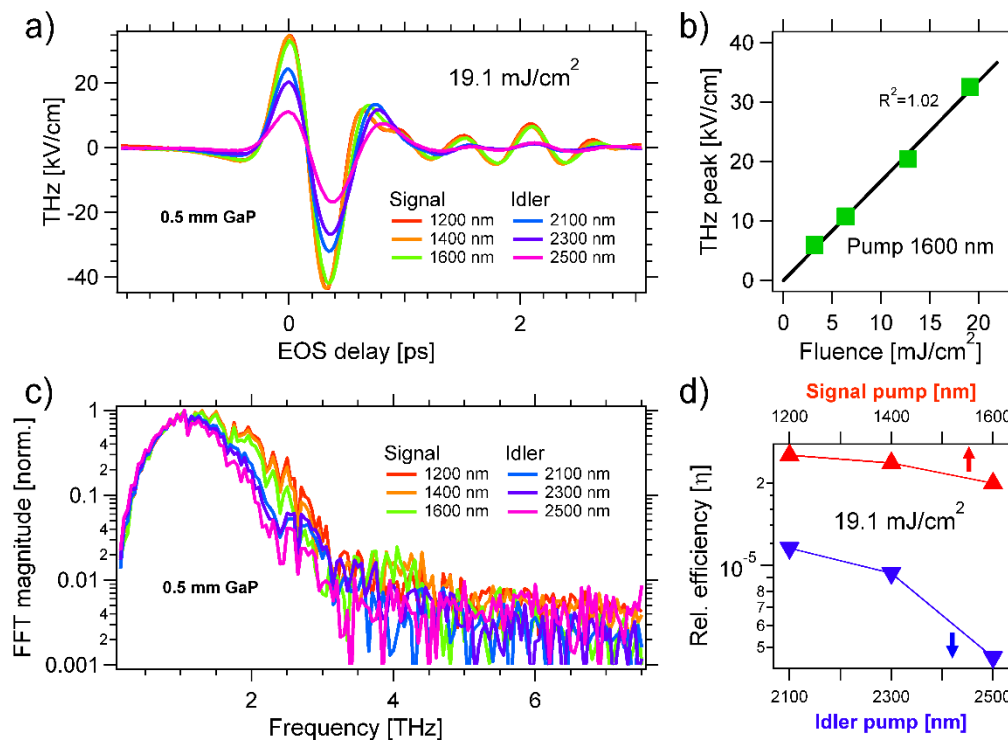


Figure 2. (a) Phase-resolved THz fields emitted by optical rectification in 0.5 mm thick GaP crystal. We use as pump pulses the output of an optical parametric amplifier between 1200 and 2500 nm. The pump fluence is set to 19.1 mJ/cm² for all pump wavelengths (λ_p). The THz is detected by electro-optical sampling (EOS) in another 0.5 mm thick gallium phosphide (GaP) crystal. We use an additional 90 fs long sampling beam at 790 nm for EOS. (b) We set the pump to $\lambda_p = 1600$ nm and plot the peak THz field value at $t_{EOS} = 0$ ps versus pump fluence. We obtain a linear fit with an R^2 value of 1.02, which confirms THz emission by a nonlinear optical process of rectification. (c) Normalized spectrum of the THz field as a function of λ_p . As expected, the frequency range is increased for shorter wavelengths [84], it is broad at $\lambda_p = 1200$ nm and narrow at $\lambda_p = 2500$ nm. (d) Estimated conversion efficiency of NIR radiation into THz radiation as a function of pump color. The efficiency is $\eta \sim 3 \times 10^{-5}$ at 1200 nm and decreases for larger λ_p .

Figure 2c displays the magnitude of the Fourier transformation (FFT) of the THz fields displayed in Figure 2a. In order to compare the different frequency components, the maximum magnitude value is normalized to one in each spectrum. We found that most of the THz radiation is emitted between 0.5 and 2.5 THz. Shorter pump wavelengths yield emission of broader THz spectra. In Figure 2d, we report the relative efficiency (η) of the energy conversion of NIR into THz radiation. We estimated this efficiency to the ratio of the THz fluence and the pump fluence. The pump fluence of 19.1 mJ/cm² was obtained from the pump spot size at the generation crystal (~ 1 mm FWHM) and the input pump power, measured with a power meter (FieldMaxII-TO PM10, Coherent). We calculated the THz fluence from the THz peak field (measured with electro-optical sampling (EOS)) and the THz spot size at the detection crystal (estimated to ~ 0.4 mm FWHM with an iris). For the 0.5 mm thick GaP, we found that η decreases for increasing pump wavelength, $\eta \sim 3 \times 10^{-5}$ at $\lambda_p = 1200$ nm and $\eta \sim 5 \times 10^{-6}$ at $\lambda_p = 2500$ nm (see Figure 2d). Please note that the value of the relative efficiency is only valid under ideal conditions. In fact, this efficiency does not include reflection losses nor the nontrivial contributions by both the wavelength-dependent pump absorption in the different generation crystals [116–118,122,123] as well as the response function of the detecting apparatus [124–126].

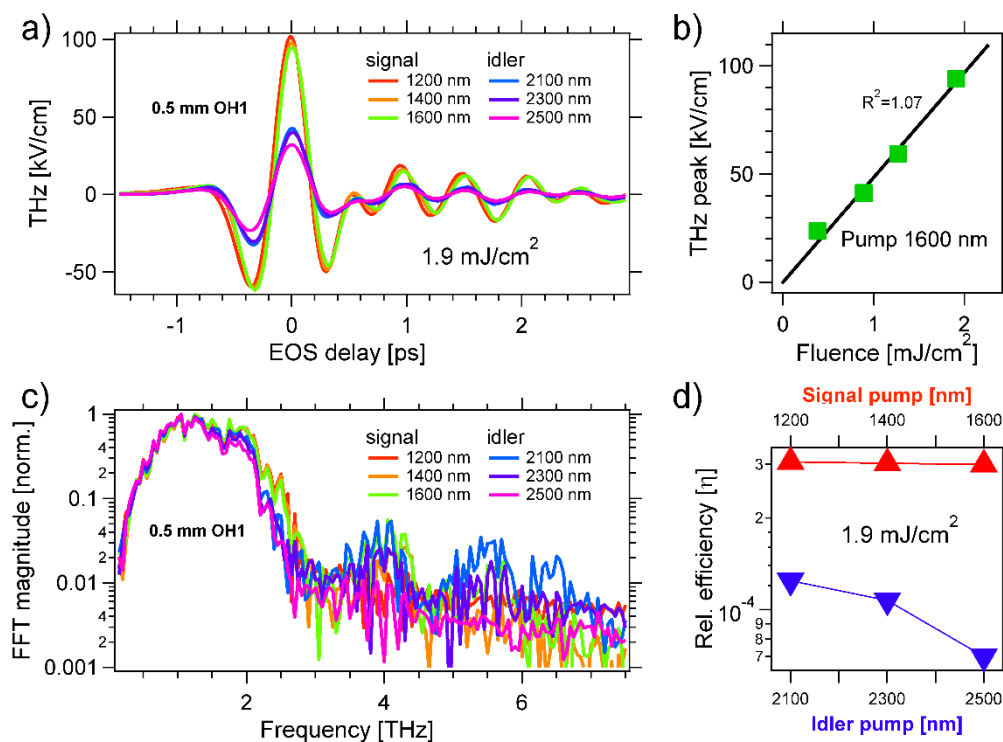


Figure 3. (a) Almost single-cycle THz fields emitted by optical rectification (OR) of optical parametric amplifier (OPA) pulses in a ~ 0.5 mm thick OH1 crystal. The pump fluence is set to 1.9 mJ/cm^2 . The THz is detected by EOS in a 0.5 mm thick GaP crystal. For EOS, we use an additional 90 fs sampling beam at 790 nm and chop the pump at 500 Hz. (b) We set the pump to $\lambda_P = 1600$ nm and detect the peak THz field at $t_{\text{EOS}} = 0$ ps versus pump fluence. A linear fit with an R^2 value of 1.07 is obtained, confirming that THz is emitted by an OR process. (c) Normalized spectrum of the THz field emitted as a function of λ_P . The spectrum has high-frequency components around ca. 4 THz and between 5 and 7 THz, that are enhanced at $\lambda_P = 2100$ nm. (d) Estimated conversion efficiency of infrared into THz radiation by OH1 as a function of λ_P . The efficiency is $\eta \sim 3 \times 10^{-4}$ between 1200 and 1600 nm, and is smaller when pumped by the idler.

3.2. 2-{3-(4-hydroxystyryl)-5,5-dimethylcyclohex-2-enylidene}malononitrile (OH1)

Figure 3a displays the THz fields generated for different pump wavelengths, all obtained at the same pump fluence of 1.9 mJ/cm^2 to avoid damaging the ~ 0.5 mm thick OH1 crystal. In all cases, we obtained almost single-cycle fields with a duration of ca. 0.3 ps (time difference between the minimum at $t_{\text{EOS}} \sim -0.15$ ps and the next minimum at $t_{\text{EOS}} \sim +0.15$ ps). A THz peak field of ~ 100 kV/cm is obtained at $t_{\text{EOS}} = 0$ ps and for $\lambda_P = 1200, 1400,$ and 1600 nm. In Figure 3b, we show the linear dependence between the THz field amplitude and the pump fluence. We set the pump wavelength to $\lambda_P = 1600$ nm and varied the fluence from 0.4 mJ/cm^2 to 1.9 mJ/cm^2 . As proved by the black line fit ($R^2 = 1.07$), a linear relationship held. Figure 3c displays the normalized magnitude of the FFT of the THz fields displayed in Figure 3a. While most of the THz radiation was emitted between 0.5 and 2 THz, additional sub-bands were found around ca. 4 THz and between 5 and 7 THz. These high frequency components were enhanced at $\lambda_P = 2100$ nm. In Figure 3d, we report the relative efficiency of the NIR-to-THz energy conversion by OH1. We found $\eta \sim 3 \times 10^{-4}$ for $\lambda_P = 1200$ nm, 1400 nm, 1600 nm. The efficiency dropped at longer wavelengths.

3.3. 4-N,N-dimethylamino-4'-N'-methyl-stilbazolium 2,4,6-trimethylbenzenesulfonate (DSTMS)

Figure 4a displays the THz fields generated via OR in DSTMS, all obtained at the same pump fluence (6.4 mJ/cm^2). For most pump wavelengths, we obtained single-cycle fields with a duration of ca. 0.27 ps (the first minimum is at $t_{\text{EOS}} \sim -0.15$ ps and the second at $t_{\text{EOS}} \sim +0.12$ ps). A THz peak

field of ~ 177 kV/cm was obtained at $t_{\text{EOS}} = 0$ ps for $\lambda_{\text{p}} = 1200$ nm, 1400 nm, 1600 nm, and 2100 nm. We chose the pump wavelength of $\lambda_{\text{p}} = 1600$ nm and varied the fluence from 0.6 mJ/cm² to 6.4 mJ/cm². The result is plotted in Figure 4b which confirms a linear relationship is found between the emitted THz field and the pump intensity, as demonstrated by the black line fit ($R^2 = 1.01$). Figure 4c displays the normalized magnitude of the FFT of the THz fields displayed in Figure 4a. We found that DSTMS emits THz radiation over a broad frequency range that spans the entire acquisition window from ca. 0.5 to 7 THz. The bandwidth of the emission spectrum was smaller at longer pump wavelengths. In Figure 4d, we report the relative efficiency of the OR nonlinear process in DSTMS. We found $\eta \sim 2 \times 10^{-4}$ for $\lambda_{\text{p}} = 1200, 1400, 1600,$ and 2100 nm. The efficiency dropped for the larger wavelengths and amounts to $\eta \sim 6 \times 10^{-5}$ at $\lambda_{\text{p}} = 2500$ nm.

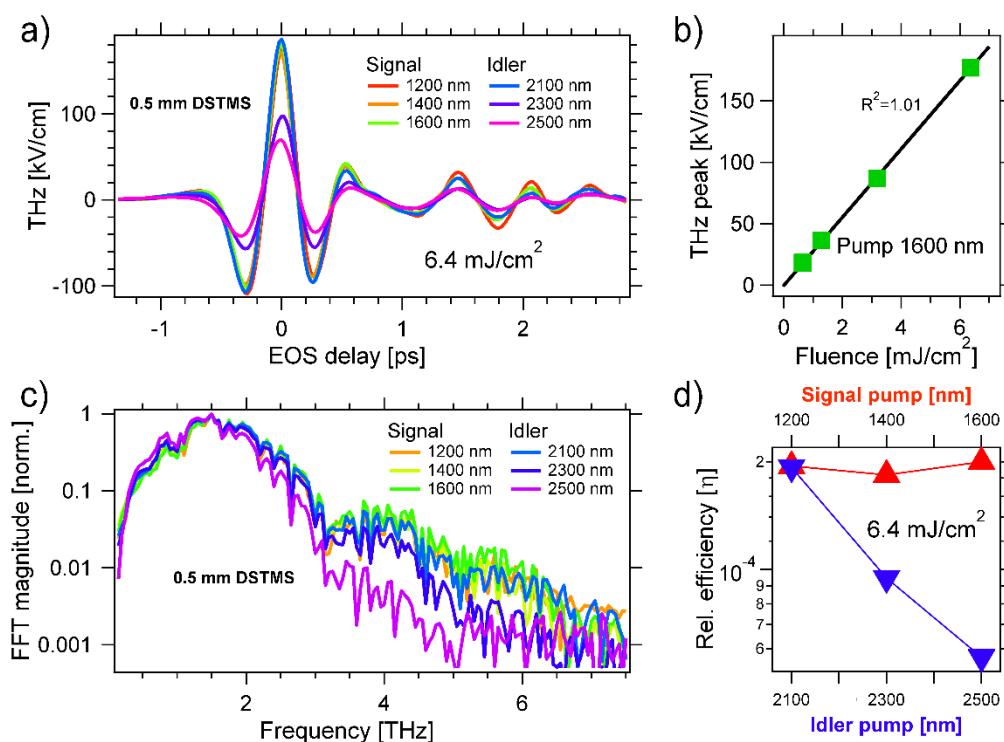


Figure 4. (a) THz emission by a ~ 0.5 mm thick 4-N,N-dimethylamino-4'-N'-methyl-stilbazolium 2,4,6-trimethylbenzenesulfonate (DSTMS) crystal. The pump fluence is set to 6.4 mJ/cm². The THz is detected by EOS, see text for details. (b) We set the pump to $\lambda_{\text{p}} = 1600$ nm, vary the pump fluence, and detect the peak THz field at $t_{\text{EOS}} = 0$ ps. We obtain a linear trend that can be fitted with an R^2 value of 1.01. (c) Normalized spectrum of the THz field generated for different pump wavelengths. The spectrum is broader in DSTMS than in either GaP (Figure 2) or OH1 (Figure 3), with high frequency components extending over the entire detectable region [126]. (d) Estimated efficiency of the THz generation in DSTMS pumped in the NIR. The efficiency, largest between 1200 and 2100 nm, and amounts to ca. $\eta \sim 2 \times 10^{-4}$.

4. Discussion

Previously, we investigated the THz emission by GaP pumped by a mode-locked oscillator tunable between 700 and 1000 nm [84]. We found that the THz emission covers a broad range at $\lambda_{\text{p}} = 900$ nm, and that the frequency range of the emitted spectrum decreases for longer pump wavelengths. The results reported in Figure 2 corroborate these earlier findings (see Figure 2c). This benchmark confirms the validity of our experimental investigation. As expected, we also found that both organic crystals are more efficient THz sources than gallium phosphide. The relative energy conversion efficiencies of GaP, OH1, and DSTMS at $\lambda_{\text{p}} = 1600$ nm are $\eta \sim 2 \times 10^{-5}$, $\eta \sim 3 \times 10^{-4}$, and $\eta \sim 2 \times 10^{-4}$, respectively.

In order to perform non-linear THz experiments on liquid water (Figure 1), broad and intense THz sources are required. The pump intensity required to drive liquid water into the nonlinear response regime depends on the wavelength. Based on the third-order responses reported previously, we tentatively estimate to 50 GW/cm², 5 TW/cm², 1 GW/cm², and 5 TW/cm², the peak power required to induce a pump-probe signal of roughly 1% at the frequency of ~1 MHz [127,128], ~1 THz [72], ~10 THz [54], and ~200 THz [129–140], respectively.

With the aim of generating such intense pump fields, here, we investigated the THz emission by organic crystals with high electro-optic coefficients and pumped by laser pulses spanning the entire OPA spectrum. Peak fields above 0.1 MV/cm were emitted by both OH1 (Figure 3) as well as DSTMS (Figure 4) for loosely focused pump pulses and fluences of only few mJ/cm². Both organic crystals also emit some radiation over the whole detection range and up to 7 THz [126], with DSTMS emitting the broadest THz spectra (Figure 4). To the best of our knowledge, here, we reported—for the first time—the THz generation by OR in OH1 and DSTMS pumped by idler beams at the wavelength $\lambda_p \geq 2100$ nm. As shown in Figure 4, we found out that DSTMS emits a broad spectrum at $\lambda_p = 2100$ nm with an unchanged high efficiency ($\eta \sim 2 \times 10^{-4}$). Thus, this crystal could generate intense THz radiation from special laser sources operating in the NIR.

Future experimental developments should aim both at scaling up the pump fluence without damaging these fragile organic crystals, as well as extending the frequency bandwidth of the detection apparatus without losing dynamical range. Pulse-shaping techniques [89,141] controlling the radiation wavefront [71,94] and/or the spatiotemporal chirp [65] of the laser beams could possibly be optimized to broaden the THz spectrum.

Author Contributions: Conceptualization, F.N. and M.H.; methodology, F.N. and B.G.; software, F.N.; validation, B.G.; formal analysis, F.N. and B.G.; investigation, B.G.; resources, F.N. and B.G.; data curation, F.N. and B.G.; writing—original draft preparation, F.N. and M.H.; writing—review and editing, F.N., B.G., and M.H.; visualization, F.N.; supervision, F.N. and M.H.; project administration, F.N. and M.H. All authors have read and agreed to the published version of the manuscript.

Funding: M.H. acknowledges funding by the ERC Advanced Grant 695437. Funded by the Deutsche Forschungsgemeinschaft (DFG, German Research Foundation) under Germany's Excellence Strategy –EXC 2033–390677874–RESOLV.

Acknowledgments: F.N. acknowledges fruitful discussions with C. Hoberg and E. Adams.

Conflicts of Interest: The authors declare no conflict of interest. The funders had no role in the design of the study; in the collection, analyses, or interpretation of data; in the writing of the manuscript, or in the decision to publish the results.

References

1. Heyden, M.; Sun, J.; Funkner, S.; Mathias, G.; Forbert, H.; Havenith, M.; Marx, D. Dissecting the THz spectrum of liquid water from first principles via correlations in time and space. *Proc. Natl. Acad. Sci. USA* **2010**, *107*, 12068–12073. [[CrossRef](#)]
2. Zelsmann, H.R. Temperature dependence of the optical constants for liquid H₂O and D₂O in the far IR region. *J. Mol. Struct.* **1995**, *350*, 95–114. [[CrossRef](#)]
3. Ellison, W.J. Permittivity of Pure Water, at Standard Atmospheric Pressure, over the Frequency Range 0–25THz and the Temperature Range 0–100 °C. *J. Phys. Chem. Ref. Data* **2007**, *36*, 1–18. [[CrossRef](#)]
4. Bertie, J.E.; Lan, Z. Infrared Intensities of Liquids XX: The Intensity of the OH Stretching Band of Liquid Water Revisited, and the Best Current Values of the Optical Constants of H₂O(l) at 25 °C between 15,000 and 1 cm⁻¹. *Appl. Spectrosc.* **1996**, *50*, 1047–1057. [[CrossRef](#)]
5. Hale, G.M.; Querry, M.R. Optical Constants of Water in the 200-nm to 200- μ m Wavelength Region. *Appl. Opt.* **1973**, *12*, 555. [[CrossRef](#)]
6. Ando, K.; Hynes, J.T. Molecular mechanism of HCl acid ionization in water: Ab initio potential energy surfaces and Monte Carlo simulations. *J. Phys. Chem. B* **1997**, *101*, 10464–10478. [[CrossRef](#)]

7. Mukherjee, A.; Lavery, R.; Bagchi, B.; Hynes, J.T. On the molecular mechanism of drug intercalation into DNA: A simulation study of the intercalation pathway, free energy, and DNA structural changes. *J. Am. Chem. Soc.* **2008**, *130*, 9747–9755. [[CrossRef](#)]
8. Wilhelm, M.; Mukherjee, A.; Bouvier, B.; Zakrzewska, K.; Hynes, J.T.; Lavery, R. Multistep drug intercalation: Molecular dynamics and free energy studies of the binding of daunomycin to DNA. *J. Am. Chem. Soc.* **2012**, *134*, 8588–8596. [[CrossRef](#)]
9. Laage, D.; Hynes, J.T. A Molecular Jump Mechanism of Water Reorientation. *Science* **2006**, *311*, 832–835. [[CrossRef](#)]
10. Kaatze, U. Water, the special liquid. *J. Mol. Liq.* **2018**, *259*, 304–318. [[CrossRef](#)]
11. Ball, P. Water—An enduring mystery. *Nature* **2008**, *452*, 291–292. [[CrossRef](#)]
12. Nilsson, A.; Pettersson, L.G.M. The structural origin of anomalous properties of liquid water. *Nat. Commun.* **2015**, *6*, 8998. [[CrossRef](#)] [[PubMed](#)]
13. Sidler, D.; Hamm, P. Feynman diagram description of 2D-Raman-THz spectroscopy applied to water. *J. Chem. Phys.* **2019**, *150*, 044202. [[CrossRef](#)] [[PubMed](#)]
14. Morgenstern, K.; Marx, D.; Havenith, M.; Muhler, M. Editorial of the PCCP themed issue on “Solvation Science”. *Phys. Chem. Chem. Phys.* **2015**, *17*, 8295–8296. [[CrossRef](#)] [[PubMed](#)]
15. Havenith, M. Solvation Science: A New Interdisciplinary Field. *Angew. Chem. Int. Ed.* **2016**, *55*, 1218–1219. [[CrossRef](#)] [[PubMed](#)]
16. Morawietz, T.; Marsalek, O.; Pattenaude, S.R.; Streacker, L.M.; Ben-Amotz, D.; Markland, T.E. The Interplay of Structure and Dynamics in the Raman Spectrum of Liquid Water over the Full Frequency and Temperature Range. *J. Phys. Chem. Lett.* **2018**, *9*, 851–857. [[CrossRef](#)]
17. Nibali, V.C.; Havenith, M.; Conti Nibali, V.; Havenith, M.; Nibali, V.C.; Havenith, M. New insights into the role of water in biological function: Studying solvated biomolecules using terahertz absorption spectroscopy in conjunction with molecular dynamics simulations. *J. Am. Chem. Soc.* **2014**, *136*, 12800–12807. [[CrossRef](#)] [[PubMed](#)]
18. Kaatze, U. The dielectric properties of water in its different states of interaction. *J. Solut. Chem.* **1997**, *26*, 1049–1112. [[CrossRef](#)]
19. Huang, W.; Richert, R. The Physics of Heating by Time-Dependent Fields: Microwaves and Water Revisited. *J. Phys. Chem. B* **2008**, *112*, 9909–9913. [[CrossRef](#)]
20. Vinh, N.Q.; Sherwin, M.S.; Allen, S.J.; George, D.K.; Rahmani, A.J.; Plaxco, K.W. High-precision gigahertz-to-terahertz spectroscopy of aqueous salt solutions as a probe of the femtosecond-to-picosecond dynamics of liquid water. *J. Chem. Phys.* **2015**, *142*, 164502. [[CrossRef](#)]
21. Popov, I.; Ben Ishai, P.; Khamzin, A.; Feldman, Y. The mechanism of the dielectric relaxation in water. *Phys. Chem. Chem. Phys.* **2016**, *18*, 13941–13953. [[CrossRef](#)] [[PubMed](#)]
22. Elton, D.C. The origin of the Debye relaxation in liquid water and fitting the high frequency excess response. *Phys. Chem. Chem. Phys.* **2017**, *19*, 18739–18749. [[CrossRef](#)] [[PubMed](#)]
23. Novelli, F.; Bernal Lopez, M.; Schwaab, G.; Roldan Cuenya, B.; Havenith, M. Water Solvation of Charged and Neutral Gold Nanoparticles. *J. Phys. Chem. B* **2019**, *123*, 6521–6528. [[CrossRef](#)] [[PubMed](#)]
24. Schienbein, P.; Schwaab, G.; Forbert, H.; Havenith, M.; Marx, D. Correlations in the Solute–Solvent Dynamics Reach Beyond the First Hydration Shell of Ions. *J. Phys. Chem. Lett.* **2017**, *8*, 2373–2380. [[CrossRef](#)]
25. Elton, D.C.; Fernández-Serra, M. The hydrogen-bond network of water supports propagating optical phonon-like modes. *Nat. Commun.* **2016**, *7*, 10193. [[CrossRef](#)]
26. Cassone, G.; Sponer, J.; Trusso, S.; Saija, F. Ab initio spectroscopy of water under electric fields. *Phys. Chem. Chem. Phys.* **2019**, *21*, 21205–21212. [[CrossRef](#)]
27. Wynne, K.; Carey, J.J. An integrated description of terahertz generation through optical rectification, charge transfer, and current surge. *Opt. Commun.* **2005**, *256*, 400–413. [[CrossRef](#)]
28. Bacon, D.R.; Burnett, A.D.; Swithenbank, M.; Russell, C.; Li, L.; Wood, C.D.; Cunningham, J.; Linfield, E.H.; Davies, A.G.; Dean, P.; et al. Free-space terahertz radiation from an emitter. *Opt. Express* **2016**, *24*, 2779–2781. [[CrossRef](#)]
29. Hoberg, C.; Balzerowski, P.; Havenith, M. Integration of a rapid scanning technique into THz time-domain spectrometers for nonlinear THz spectroscopy measurements. *AIP Adv.* **2019**, *9*, 035348. [[CrossRef](#)]

30. Wirtz, H.; Schäfer, S.; Hoberg, C.; Havenith, M. Differences in Hydration Structure Around Hydrophobic and Hydrophilic Model Peptides Probed by THz Spectroscopy. *J. Infrared Millim. Terahertz Waves* **2018**, *39*, 816–827. [[CrossRef](#)]
31. Acbas, G.; Niessen, K.A.; Snell, E.H.; Markelz, A.G. Optical measurements of long-range protein vibrations. *Nat. Commun.* **2014**, *5*, 3076. [[CrossRef](#)] [[PubMed](#)]
32. Wu, Q.; Zhang, X.-C. Free-space electro-optic sampling of terahertz beams. *Appl. Phys. Lett.* **1995**, *67*, 3523–3525. [[CrossRef](#)]
33. Grischkowsky, D.; Keiding, S.; van Exter, M.; Fattinger, C. Far-infrared time-domain spectroscopy with terahertz beams of dielectrics and semiconductors. *J. Opt. Soc. Am. B* **1990**, *7*, 2006. [[CrossRef](#)]
34. Knippels, G.M.H.; van der Meer, A.F.G.; Mols, R.F.X.A.M.; Oepts, D.; van Amersfoort, P.W. Formation of multiple subpulses in a free-electron laser operating in the limit-cycle mode. *Phys. Rev. E* **1996**, *53*, 2778–2786. [[CrossRef](#)] [[PubMed](#)]
35. Knippels, G.M.; van der Meer, A.F. FEL diagnostics and user control. *Nucl. Instrum. Methods Phys. Res. Sect. B Beam Interact. Mater. Atoms* **1998**, *144*, 32–39. [[CrossRef](#)]
36. Knippels, G.M.H.; Mols, R.F.X.A.M.; van der Meer, A.F.G.; Oepts, D.; van Amersfoort, P.W. Intense Far-Infrared Free-Electron Laser Pulses with a Length of Six Optical Cycles. *Phys. Rev. Lett.* **1995**, *75*, 1755–1758. [[CrossRef](#)]
37. Casalbuoni, S.; Schlarb, H.; Schmidt, B.; Schmüser, P.; Steffen, B.; Winter, A. Numerical studies on the electro-optic detection of femtosecond electron bunches. *Phys. Rev. Spec. Top. Accel. Beams* **2008**, *11*, 072802. [[CrossRef](#)]
38. Kawase, K.; Kato, R.; Irizawa, A.; Fujimoto, M.; Kashiwagi, S.; Yamamoto, S.; Kamitsukasa, F.; Osumi, H.; Yaguchi, M.; Tokuchi, A.; et al. The high-power operation of a terahertz free-electron laser based on a normal conducting RF linac using beam conditioning. *Nucl. Instrum. Methods Phys. Res. Sect. A Accel. Spectrometers Detect. Assoc. Equip.* **2013**, *726*, 96–103. [[CrossRef](#)]
39. Adhlakha, N.; Di Pietro, P.; Piccirilli, F.; Cinquegrana, P.; Di Mitri, S.; Sigalotti, P.; Spampinati, S.; Veronese, M.; Lupi, S.; Perucchi, A. The TeraFERMI Electro-Optic Sampling Set-Up for Fluence-Dependent Spectroscopic Measurements. *Condens. Matter* **2020**, *5*, 8. [[CrossRef](#)]
40. Di Mitri, S.; Perucchi, A.; Adhlakha, N.; Di Pietro, P.; Nicastro, S.; Roussel, E.; Spampinati, S.; Veronese, M.; Allaria, E.; Badano, L.; et al. Coherent THz Emission Enhanced by Coherent Synchrotron Radiation Wakefield. *Sci. Rep.* **2018**, *8*, 11661. [[CrossRef](#)]
41. Neil, G.R. Accelerator Sources for THz Science: A Review. *J. Infrared Millim. Terahertz Waves* **2014**, *35*, 5–16. [[CrossRef](#)]
42. Tan, P.; Huang, J.; Liu, K.; Xiong, Y.; Fan, M. Terahertz radiation sources based on free electron lasers and their applications. *Sci. China Inf. Sci.* **2012**, *55*, 1–15. [[CrossRef](#)]
43. Kovalev, S.; Wang, Z.; Deinert, J.-C.; Awari, N.; Chen, M.; Green, B.; Germanskiy, S.; de Oliveira, T.V.A.G.; Lee, J.S.; Deac, A.; et al. Selective THz control of magnetic order: New opportunities from superradiant undulator sources. *J. Phys. D. Appl. Phys.* **2018**, *51*, 114007. [[CrossRef](#)]
44. Stojanovic, N.; Drescher, M. Accelerator- and laser-based sources of high-field terahertz pulses. *J. Phys. B At. Mol. Opt. Phys.* **2013**, *46*, 192001. [[CrossRef](#)]
45. Shevchenko, O.A.; Melnikov, A.R.; Tararyshkin, S.V.; Getmanov, Y.V.; Serednyakov, S.S.; Bykov, E.V.; Kubarev, V.V.; Fedin, M.V.; Veber, S.L. Electronic Modulation of THz Radiation at NovoFEL: Technical Aspects and Possible Applications. *Materials* **2019**, *12*, 3063. [[CrossRef](#)]
46. Green, B.; Kovalev, S.; Asgekar, V.; Geloni, G.; Lehnert, U.; Golz, T.; Kuntzsch, M.; Bauer, C.; Hauser, J.; Voigtlaender, J.; et al. High-Field High-Repetition-Rate Sources for the Coherent THz Control of Matter. *Sci. Rep.* **2016**, *6*, 22256. [[CrossRef](#)]
47. Regensburger, S.; Mittendorff, M.; Winnerl, S.; Lu, H.; Gossard, A.C.; Preu, S. Broadband THz detection from 01 to 22 THz with large area field-effect transistors. *Opt. Express* **2015**, *23*, 20732. [[CrossRef](#)]
48. Lee, J.S.; Gensch, M.; Hinrichs, K.; Seidel, W.; Schade, U. Determination of the polarization characteristics of the ELBE free electron laser. *Infrared Phys. Technol.* **2008**, *51*, 537–540. [[CrossRef](#)]
49. Klopff, J.M.; Zvyagin, S.; Helm, M.; Kehr, S.C.; Lehnert, U.; Michel, P.; Pashkin, A.; Schneider, H.; Seide, W.; Winnerl, S. FELBE -Upgrades and Status of the IRITHz FEL User Facility at HZDR. In Proceedings of the 2018 43rd International Conference on Infrared, Millimeter, and Terahertz Waves (IRMMW-THz), Nagoya, Japan, 9–14 September 2018; IEEE: Piscataway, NJ, USA, 2018; pp. 1–2.

50. Klopff, J.M.; Greer, A.; Gubeli, J.; Neil, G.R.; Shinn, M.; Siggins, T.; Waldman, D.; Williams, G.P.; Todd, A.; Christina, V.; et al. The Jefferson Lab high power THz user facility. *Nucl. Instrum. Methods Phys. Res. Sect. A Accel. Spectrometers Detect. Assoc. Equip.* **2007**, *582*, 114–116. [[CrossRef](#)]
51. Pan, R.; Zapolnova, E.; Golz, T.; Krmpot, A.J.; Rabasovic, M.D.; Petrovic, J.; Asgekar, V.; Faatz, B.; Tavella, F.; Perucchi, A.; et al. Photon diagnostics at the FLASH THz beamline. *J. Synchrotron Radiat.* **2019**, *26*, 700–707. [[CrossRef](#)]
52. Di Pietro, P.; Adhlakha, N.; Piccirilli, F.; Capasso, L.; Svetina, C.; Di Mitri, S.; Veronese, M.; Giorgianni, F.; Lupi, S.; Perucchi, A. TeraFERMI: A Superradiant Beamline for THz Nonlinear Studies at the FERMI Free Electron Laser Facility. *Synchrotron Radiat. News* **2017**, *30*, 36–39. [[CrossRef](#)]
53. Bründermann, E.; Hübers, H.-W.; Kimmitt, M.F. *Terahertz Techniques*; Springer Series in Optical Sciences; Springer: Berlin/Heidelberg, Germany, 2012; Volume 151, ISBN 978-3-642-02591-4.
54. Novelli, F.; Pestana, L.R.; Bennett, K.C.; Dessmann, N.; Sebastiani, F.; Adams, E.M.; Ilkhchy, K.S.; Stavrias, N.; Eless, V.; Ockelmann, T.; et al. Strong Anisotropy in Liquid Water upon Librational Excitation using Terahertz Laser Fields. *arXiv* **2018**, arXiv:1809.04261.
55. Seifert, T.; Jaiswal, S.; Martens, U.; Hannegan, J.; Braun, L.; Maldonado, P.; Freimuth, F.; Kronenberg, A.; Henrizi, J.; Radu, I.; et al. Efficient metallic spintronic emitters of ultrabroadband terahertz radiation. *Nat. Photonics* **2016**, *10*, 483–488. [[CrossRef](#)]
56. Seifert, T.; Jaiswal, S.; Sajadi, M.; Jakob, G.; Winnerl, S.; Wolf, M.; Kläui, M.; Kampfrath, T. Ultrabroadband single-cycle terahertz pulses with peak fields of 300 kV cm⁻¹ from a metallic spintronic emitter. *Appl. Phys. Lett.* **2017**, *110*, 252402. [[CrossRef](#)]
57. Oh, T.I.; You, Y.S.; Jhajj, N.; Rosenthal, E.W.; Milchberg, H.M.; Kim, K.Y. Intense terahertz generation in two-color laser filamentation: Energy scaling with terawatt laser systems. *New J. Phys.* **2013**, *15*, 075002. [[CrossRef](#)]
58. Kuk, D.; Yoo, Y.J.; Rosenthal, E.W.; Jhajj, N.; Milchberg, H.M.; Kim, K.Y. Generation of scalable terahertz radiation from cylindrically focused two-color laser pulses in air. *Appl. Phys. Lett.* **2016**, *108*. [[CrossRef](#)]
59. Dey, I.; Jana, K.; Fedorov, V.Y.; Koulouklidis, A.D.; Mondal, A.; Shaikh, M.; Sarkar, D.; Lad, A.D.; Tzortzakis, S.; Couairon, A.; et al. Highly efficient broadband terahertz generation from ultrashort laser filamentation in liquids. *Nat. Commun.* **2017**, *8*, 1184. [[CrossRef](#)]
60. Koulouklidis, A.D.; Gollner, C.; Shumakova, V.; Fedorov, V.Y.; Pugžlys, A.; Baltuška, A.; Tzortzakis, S. Observation of extremely efficient terahertz generation from mid-infrared two-color laser filaments. *Nat. Commun.* **2020**, *11*, 292. [[CrossRef](#)]
61. Boyd, R.W. *Nonlinear Optics*, 3rd ed.; Academic Press: Cambridge, MA, USA, 2007; ISBN 978-0-12-369470-6.
62. Fülöp, J.A.; Pálfalvi, L.; Klingebiel, S.; Almási, G.; Krausz, F.; Karsch, S.; Hebling, J. Generation of sub-mJ terahertz pulses by optical rectification. *Opt. Lett.* **2012**, *37*, 557. [[CrossRef](#)]
63. Vicario, C.; Ovchinnikov, A.V.; Ashitkov, S.I.; Agranat, M.B.; Fortov, V.E.; Hauri, C.P. Generation of 09-mJ THz pulses in DSTMS pumped by a Cr:Mg₂SiO₄ laser. *Opt. Lett.* **2014**, *39*, 6632. [[CrossRef](#)]
64. Sell, A.; Leitenstorfer, A.; Huber, R. Phase-locked generation and field-resolved detection of widely tunable terahertz pulses with amplitudes exceeding 100 MV/cm. *Opt. Lett.* **2008**, *33*, 2767. [[CrossRef](#)] [[PubMed](#)]
65. Liu, B.; Bromberger, H.; Cartella, A.; Gebert, T.; Först, M.; Cavalleri, A. Generation of narrowband, high-intensity, carrier-envelope phase-stable pulses tunable between 4 and 18 THz. *Opt. Lett.* **2017**, *42*, 129. [[CrossRef](#)] [[PubMed](#)]
66. Huang, W.R.; Huang, S.-W.; Granados, E.; Ravi, K.; Hong, K.-H.; Zapata, L.E.; Kärtner, F.X. Highly efficient terahertz pulse generation by optical rectification in stoichiometric and cryo-cooled congruent lithium niobate. *J. Mod. Opt.* **2014**, *0340*, 1–8. [[CrossRef](#)]
67. Hirori, H.; Doi, A.; Blanchard, F.; Tanaka, K. Single-cycle terahertz pulses with amplitudes exceeding 1 MV/cm generated by optical rectification in LiNbO₃. *Appl. Phys. Lett.* **2011**, *98*, 091106. [[CrossRef](#)]
68. Jewariya, M.; Nagai, M.; Tanaka, K. Enhancement of terahertz wave generation by cascaded $\chi^{(2)}$ processes in LiNbO₃. *J. Opt. Soc. Am. B* **2009**, *26*, A101. [[CrossRef](#)]
69. Hirori, H.; Doi, A.; Blanchard, F.; Tanaka, K. Erratum: “Single-cycle terahertz pulses with amplitudes exceeding 1 MV/cm generated by optical rectification in LiNbO₃” [*Appl. Phys. Lett.* **98**, 091106 (2011)]. *Appl. Phys. Lett.* **2013**, *103*, 259901. [[CrossRef](#)]
70. Yeh, K.-L.; Hebling, J.; Hoffmann, M.C.; Nelson, K.A. Generation of high average power 1 kHz shaped THz pulses via optical rectification. *Opt. Commun.* **2008**, *281*, 3567–3570. [[CrossRef](#)]

71. Hebling, J.; Yeh, K.-L.; Hoffmann, M.C.; Bartal, B.; Nelson, K.A. Generation of high-power terahertz pulses by tilted-pulse-front excitation and their application possibilities. *J. Opt. Soc. Am. B* **2008**, *25*, B6. [[CrossRef](#)]
72. Zalden, P.; Song, L.; Wu, X.; Huang, H.; Ahr, F.; Mücke, O.D.; Reichert, J.; Thorwart, M.; Mishra, P.K.; Welsch, R.; et al. Molecular polarizability anisotropy of liquid water revealed by terahertz-induced transient orientation. *Nat. Commun.* **2018**, *9*, 2142. [[CrossRef](#)]
73. Novelli, F.; Chon, J.W.M.; Davis, J.A. Terahertz thermometry of gold nanospheres in water. *Opt. Lett.* **2016**, *41*, 5801. [[CrossRef](#)]
74. Novelli, F.; Ostovar Pour, S.; Tollerud, J.; Roozbeh, A.; Appadoo, D.R.T.T.; Blanch, E.W.; Davis, J.A. Time-Domain THz Spectroscopy Reveals Coupled Protein–Hydration Dielectric Response in Solutions of Native and Fibrils of Human Lysozyme. *J. Phys. Chem. B* **2017**, *121*, 4810–4816. [[CrossRef](#)] [[PubMed](#)]
75. Novelli, F.; Fausti, D.; Giusti, F.; Parmigiani, F.; Hoffmann, M. Mixed regime of light-matter interaction revealed by phase sensitive measurements of the dynamical Franz-Keldysh effect. *Sci. Rep.* **2013**, *3*, 1227. [[CrossRef](#)] [[PubMed](#)]
76. Balčytis, A.; Ryu, M.; Wang, X.; Novelli, F.; Seniutinas, G.; Du, S.; Wang, X.; Li, J.; Davis, J.; Appadoo, D.; et al. Silk: Optical Properties over 12.6 Octaves THz-IR-Visible-UV Range. *Materials* **2017**, *10*, 356. [[CrossRef](#)] [[PubMed](#)]
77. Meyer, F.; Vogel, T.; Ahmed, S.; Saraceno, C.J. Single-cycle, MHz-repetition rate THz source with 66 mW of average power. *arXiv* **2020**, arXiv:2002.00222. [[CrossRef](#)]
78. Huber, R.; Brodschelm, A.; Tauser, F.; Leitenstorfer, A. Generation and field-resolved detection of femtosecond electromagnetic pulses tunable up to 41 THz. *Appl. Phys. Lett.* **2000**, *76*, 3191–3193. [[CrossRef](#)]
79. Kübler, C.; Huber, R.; Tübel, S.; Leitenstorfer, A. Ultrabroadband detection of multi-terahertz field transients with GaSe electro-optic sensors: Approaching the near infrared. *Appl. Phys. Lett.* **2004**, *85*, 3360–3362. [[CrossRef](#)]
80. Junginger, F.; Sell, A.; Schubert, O.; Mayer, B.; Brida, D.; Marangoni, M.; Cerullo, G.; Leitenstorfer, A.; Huber, R. Single-cycle multiterahertz transients with peak fields above 10 MV/cm. *Opt. Lett.* **2010**, *35*, 2645. [[CrossRef](#)]
81. Blanchard, F.; Sharma, G.; Razzari, L.; Ropagnol, X.; Bandulet, H.C.; Vidal, F.; Morandotti, R.; Kieffer, J.C.; Ozaki, T.; Tiedje, H.; et al. Generation of intense terahertz radiation via optical methods. *IEEE J. Sel. Top. Quantum Electron.* **2011**, *17*, 5–16. [[CrossRef](#)]
82. Blanchard, F.; Razzari, L.; Bandulet, H.C.; Sharma, G.; Morandotti, R.; Kieffer, J.C.; Ozaki, T.; Reid, M.; Tiedje, H.F.; Haugen, H.K.; et al. Generation of 1.5 μ J single-cycle terahertz pulses by optical rectification from a large aperture ZnTe crystal. *Opt. Express* **2007**, *15*, 13212. [[CrossRef](#)]
83. Knorr, M.; Raab, J.; Tauer, M.; Merkl, P.; Peller, D.; Wittmann, E.; Riedle, E.; Lange, C.; Huber, R. Phase-locked multi-terahertz electric fields exceeding 13 MV/cm at a 190 kHz repetition rate. *Opt. Lett.* **2017**, *42*, 4367. [[CrossRef](#)]
84. Aoki, K.; Savolainen, J.; Havenith, M. Broadband terahertz pulse generation by optical rectification in GaP crystals. *Appl. Phys. Lett.* **2017**, *110*, 201103. [[CrossRef](#)]
85. Shalit, A.; Ahmed, S.; Savolainen, J.; Hamm, P. Terahertz echoes reveal the inhomogeneity of aqueous salt solutions. *Nat. Chem.* **2017**, *9*, 273–278. [[CrossRef](#)] [[PubMed](#)]
86. Savolainen, J.; Ahmed, S.; Hamm, P. Two-dimensional Raman-terahertz spectroscopy of water. *Proc. Natl. Acad. Sci. USA* **2013**, *110*, 20402–20407. [[CrossRef](#)] [[PubMed](#)]
87. Savolainen, J.; Uhlig, F.; Ahmed, S.; Hamm, P.; Jungwirth, P. Direct observation of the collapse of the delocalized excess electron in water. *Nat. Chem.* **2014**, *6*, 697–701. [[CrossRef](#)]
88. Meyer, F.; Hekmat, N.; Vogel, T.; Omar, A.; Mansourzadeh, S.; Fobbe, F.; Hoffmann, M.; Wang, Y.; Saraceno, C.J. Milliwatt-class broadband THz source driven by a 112 W, sub-100 fs thin-disk laser. *Opt. Express* **2019**, *27*, 30340. [[CrossRef](#)]
89. Somma, C.; Folpini, G.; Gupta, J.; Reimann, K.; Woerner, M.; Elsaesser, T. Ultra-broadband terahertz pulses generated in the organic crystal DSTMS. *Opt. Lett.* **2015**, *40*, 3404. [[CrossRef](#)]
90. Houver, S.; Huber, L.; Savoini, M.; Abreu, E.; Johnson, S.L. 2D THz spectroscopic investigation of ballistic conduction-band electron dynamics in InSb. *Opt. Express* **2019**, *27*, 10854. [[CrossRef](#)]
91. Finneran, I.A.; Welsch, R.; Allodi, M.A.; Miller, T.F.; Blake, G.A. Coherent two-dimensional terahertz-terahertz-Raman spectroscopy. *Proc. Natl. Acad. Sci. USA* **2016**, *113*, 6857–6861. [[CrossRef](#)]

92. Chefonov, O.V.; Ovchinnikov, A.V.; Agranat, M.B.; Stepanov, A.N. Terahertz beam spot size measurements by a CCD camera. *Opt. Lett.* **2019**, *44*, 4099. [[CrossRef](#)]
93. Chefonov, O.V.; Ovchinnikov, A.V.; Hauri, C.P.; Agranat, M.B. Broadband and narrowband laser-based terahertz source and its application for resonant and non-resonant excitation of antiferromagnetic modes in NiO. *Opt. Express* **2019**, *27*, 27273. [[CrossRef](#)]
94. Shalaby, M.; Hauri, C.P. Demonstration of a low-frequency three-dimensional terahertz bullet with extreme brightness. *Nat. Commun.* **2015**, *6*, 5976. [[CrossRef](#)] [[PubMed](#)]
95. Majkić, A.; Zgonik, M.; Petelin, A.; Jazbinšek, M.; Ruiz, B.; Medrano, C.; Günter, P. Terahertz source at 9.4 THz based on a dual-wavelength infrared laser and quasi-phase matching in organic crystals OH1. *Appl. Phys. Lett.* **2014**, *105*, 1–5. [[CrossRef](#)]
96. Brenier, A. Two-frequency pulsed YLiF₄:Nd lasing out of the principal axes and THz generation. *Opt. Lett.* **2015**, *40*, 4496. [[CrossRef](#)]
97. Giorgianni, F.; Cea, T.; Vicario, C.; Hauri, C.P.; Withanage, W.K.; Xi, X.; Benfatto, L. Leggett mode controlled by light pulses. *Nat. Phys.* **2019**, *15*, 341–346. [[CrossRef](#)]
98. Monoszlai, B.; Vicario, C.; Jazbinsek, M.; Hauri, C.P. High-energy terahertz pulses from organic crystals: DAST and DSTMS pumped at Ti:sapphire wavelength. *Opt. Lett.* **2013**, *38*, 5106. [[CrossRef](#)] [[PubMed](#)]
99. Sajadi, M.; Wolf, M.; Kampfrath, T. Transient birefringence of liquids induced by terahertz electric-field torque on permanent molecular dipoles. *Nat. Commun.* **2017**, *8*, 14963. [[CrossRef](#)] [[PubMed](#)]
100. Savoini, M.; Huber, L.; Cuppen, H.; Abreu, E.; Kubli, M.; Neugebauer, M.J.; Duan, Y.; Beaud, P.; Xu, J.; Rasing, T.; et al. THz Generation and Detection by Fluorenone Based Organic Crystals. *ACS Photonics* **2018**, *5*, 671–677. [[CrossRef](#)]
101. Vicario, C.; Monoszlai, B.; Jazbinsek, M.; Lee, S.H.; Kwon, O.P.; Hauri, C.P. Intense, carrier frequency and bandwidth tunable quasi single-cycle pulses from an organic emitter covering the Terahertz frequency gap. *Sci. Rep.* **2015**, *5*, 1–8. [[CrossRef](#)]
102. Giorgianni, F.; Puc, U.; Jazbinsek, M.; Cea, T.; Koo, M.-J.; Han, J.-H.; Kwon, O.-P.; Vicario, C. Supercontinuum generation in OHQ-N2S organic crystal driven by intense terahertz fields. *Opt. Lett.* **2019**, *44*, 4881. [[CrossRef](#)]
103. Vieweg, N.; Rettich, F.; Deninger, A.; Roehle, H.; Dietz, R.; Göbel, T.; Schell, M. Terahertz-time domain spectrometer with 90 dB peak dynamic range. *J. Infrared Millim. Terahertz Waves* **2014**, *35*, 823–832. [[CrossRef](#)]
104. Kohlhaas, R.B.; Breuer, S.; Nellen, S.; Liebermeister, L.; Schell, M.; Semtsiv, M.P.; Masselink, W.T.; Globisch, B. Photoconductive terahertz detectors with 105 dB peak dynamic range made of rhodium doped InGaAs. *Appl. Phys. Lett.* **2019**, *114*, 221103. [[CrossRef](#)]
105. Blanchard, F.; Tanaka, K. Improving time and space resolution in electro-optic sampling for near-field terahertz imaging. *Opt. Lett.* **2016**, *41*, 4645. [[CrossRef](#)] [[PubMed](#)]
106. Han, P.Y.; Tani, M.; Pan, F.; Zhang, X.-C. Use of the organic crystal DAST for terahertz beam applications. *Opt. Lett.* **2000**, *25*, 675. [[CrossRef](#)] [[PubMed](#)]
107. Schneider, A.; Biaggio, I.; Günter, P. Terahertz-induced lensing and its use for the detection of terahertz pulses in a birefringent crystal. *Appl. Phys. Lett.* **2004**, *84*, 2229–2231. [[CrossRef](#)]
108. Schneider, A.; Günter, P. Coherent detection of terahertz pulses based on two-photon absorption in a photodiode. *Appl. Phys. Lett.* **2007**, *90*. [[CrossRef](#)]
109. Martin, M.; Mangeney, J.; Crozat, P.; Mounaix, P. Optical phase detection in a 4-N,N-dimethylamino-4'-N-methyl-stilbazolium tosylate crystal for terahertz time domain spectroscopy system at 1.55 μm wavelength. *Appl. Phys. Lett.* **2010**, *97*, 1–4. [[CrossRef](#)]
110. Ilyakov, I.E.; Kitaeva, G.K.; Shishkin, B.V.; Akhmedzhanov, R.A. The use of DSTMS crystal for broadband terahertz electro-optic sampling based on laser pulse amplitude changes. *Laser Phys. Lett.* **2018**, *15*, 125401. [[CrossRef](#)]
111. Lu, X.; Zhang, X.-C. Balanced terahertz wave air-biased-coherent-detection. *Appl. Phys. Lett.* **2011**, *98*, 151111. [[CrossRef](#)]
112. Lu, X.; Zhang, X.-C. Investigation of ultra-broadband terahertz time-domain spectroscopy with terahertz wave gas photonics. *Front. Optoelectron.* **2014**, *7*, 121–155. [[CrossRef](#)]
113. Wang, T.; Iwaszczuk, K.; Wrisberg, E.A.; Denning, E.V.; Jepsen, P.U. Linearity of Air-Biased Coherent Detection for Terahertz Time-Domain Spectroscopy. *J. Infrared Millim. Terahertz Waves* **2016**, *37*, 592–604. [[CrossRef](#)]

114. Skoromets, V.; Němec, H.; Goian, V.; Kamba, S.; Kužel, P. Performance Comparison of Time-Domain Terahertz, Multi-terahertz, and Fourier Transform Infrared Spectroscopies. *J. Infrared Millim. Terahertz Waves* **2018**, *39*, 1249–1263. [[CrossRef](#)]
115. Lewis, R.A. A review of terahertz detectors. *J. Phys. D. Appl. Phys.* **2019**, *52*, 433001. [[CrossRef](#)]
116. Hunziker, C.; Kwon, S.-J.; Figi, H.; Juvalta, F.; Kwon, O.-P.; Jazbinsek, M.; Günter, P. Configurationally locked, phenolic polyene organic crystal 2-(3-(4-hydroxystyryl)-5,5-dimethylcyclohex-2-enylidene)malononitrile: Linear and nonlinear optical properties. *J. Opt. Soc. Am. B* **2008**, *25*, 1678. [[CrossRef](#)]
117. Mutter, L.; Brunner, F.D.; Yang, Z.; Jazbinšek, M.; Günter, P. Linear and nonlinear optical properties of the organic crystal DSTMS. *J. Opt. Soc. Am. B* **2007**, *24*, 2556. [[CrossRef](#)]
118. Yang, Z.; Mutter, L.; Stillhart, M.; Ruiz, B.; Aravazhi, S.; Jazbinsek, M.; Schneider, A.; Gramlich, V.; Günter, P. Large-Size Bulk and Thin-Film Stilbazolium-Salt Single Crystals for Nonlinear Optics and THz Generation. *Adv. Funct. Mater.* **2007**, *17*, 2018–2023. [[CrossRef](#)]
119. Dean, N. *Electronic and Structural Dynamics of Complex Materials*; University of Oxford: Oxford, UK, 2010.
120. Lin, S.; Yu, S.; Talbayev, D. Measurement of Quadratic Terahertz Optical Nonlinearities Using Second-Harmonic Lock-in Detection. *Phys. Rev. Appl.* **2018**, *10*, 044007. [[CrossRef](#)]
121. Nemoto, N.; Higuchi, T.; Kanda, N.; Konishi, K.; Kuwata-Gonokami, M. Highly precise and accurate terahertz polarization measurements based on electro-optic sampling with polarization modulation of probe pulses. *Opt. Express* **2014**, *22*, 17915. [[CrossRef](#)] [[PubMed](#)]
122. Stillhart, M.; Schneider, A.; Günter, P. Optical properties of 4-N,N-dimethylamino-4'-N'-methyl-stilbazolium 2,4,6-trimethylbenzenesulfonate crystals at terahertz frequencies. *J. Opt. Soc. Am. B* **2008**, *25*, 1914. [[CrossRef](#)]
123. Jazbinsek, M.; Puc, U.; Abina, A.; Zidansek, A. Organic Crystals for THz Photonics. *Appl. Sci.* **2019**, *9*, 882. [[CrossRef](#)]
124. Xu, J.; Globisch, B.; Hofer, C.; Lilienfein, N.; Butler, T.; Karpowicz, N.; Pupeza, I. Three-octave terahertz pulses from optical rectification of 20 fs, 1 μm , 78 MHz pulses in GaP. *J. Phys. B At. Mol. Opt. Phys.* **2018**, *51*, 154002. [[CrossRef](#)]
125. Leitenstorfer, A.; Hunsche, S.; Shah, J.; Nuss, M.C.; Knox, W.H. Detectors and sources for ultrabroadband electro-optic sampling: Experiment and theory. *Appl. Phys. Lett.* **1999**, *74*, 1516–1518. [[CrossRef](#)]
126. Wu, Q.; Zhang, X.-C. 7 terahertz broadband GaP electro-optic sensor. *Appl. Phys. Lett.* **1997**, *70*, 1784–1786. [[CrossRef](#)]
127. Novac, B.M.; Banakhr, F.A.; Smith, I.R.; Pecastaing, L.; Ruscassie, R.; De Ferron, A.S.; Pignolet, P. Determination of the Kerr Constant of Water at 658 nm for Pulsed Intense Electric Fields. *IEEE Trans. Plasma Sci.* **2012**, *40*, 2480–2490. [[CrossRef](#)]
128. Khanna, R.K.; Dempsey, E.; Parry Jones, G. Kerr constant of water from 280 to 350 K at 632.8 nm. *Chem. Phys. Lett.* **1978**, *53*, 542–544. [[CrossRef](#)]
129. Wilkes, Z.W.; Varma, S.; Chen, Y.H.; Milchberg, H.M.; Jones, T.G.; Ting, A. Direct measurements of the nonlinear index of refraction of water at 815 and 407 nm using single-shot supercontinuum spectral interferometry. *Appl. Phys. Lett.* **2009**, *94*, 1–4. [[CrossRef](#)]
130. Harrison, N.J.; Jennings, B.R. Laser-Induced Kerr Constants for Pure Liquids. *J. Phys. Chem. Ref. Data* **1992**, *21*, 157–163. [[CrossRef](#)]
131. Shcheslavskiy, V.; Petrov, G.; Yakovlev, V.V. Nonlinear optical susceptibility measurements of solutions using third-harmonic generation on the interface. *Appl. Phys. Lett.* **2003**, *82*, 3982–3984. [[CrossRef](#)]
132. Barille, R.; Canioni, L.; Sarger, L.; Rivoire, G. Nonlinearity measurements of thin films by third-harmonic-generation microscopy. *Phys. Rev. E* **2002**, *66*, 067602. [[CrossRef](#)] [[PubMed](#)]
133. Harrison, N.J.; Jennings, B.R. Laser-induced birefringence measurement for pure liquids. *Meas. Sci. Technol.* **1992**, *3*, 120–125. [[CrossRef](#)]
134. Clay, O.; Schaffer, C.B.; Squier, J.A.; Kleinfeld, D. Ultrafast Third Harmonic Micro-Spectroscopy Reveals a Two-Photon Resonance in Human Hemoglobin. In *Proceedings of the SPIE Commercial and Biomedical Applications of Ultrafast Lasers VI*; Neev, J., Nolte, S., Heisterkamp, A., Schaffer, C.B., Eds.; SPIE: Bellingham, WA, USA, 2006; Volume 6008, p. 610809.
135. Brodeur, A.; Chin, S.L. Band-Gap Dependence of the Ultrafast White-Light Continuum. *Phys. Rev. Lett.* **1998**, *80*, 4406–4409. [[CrossRef](#)]

136. Nibbering, E.T.J.; Franco, M.A.; Prade, B.S.; Grillon, G.; Le Blanc, C.; Mysyrowicz, A. Measurement of the nonlinear refractive index of transparent materials by spectral analysis after nonlinear propagation. *Opt. Commun.* **1995**, *119*, 479–484. [[CrossRef](#)]
137. Liu, W.; Kosareva, O.; Golubtsov, I.S.; Iwasaki, A.; Becker, A.; Kandidov, V.P.; Chin, S.L. Femtosecond laser pulse filamentation versus optical breakdown in H₂O. *Appl. Phys. B Lasers Opt.* **2003**, *76*, 215–229. [[CrossRef](#)]
138. Ho, P.P.; Alfano, R.R. Optical Kerr effect in liquids. *Phys. Rev. A* **1979**, *20*, 2170–2187. [[CrossRef](#)]
139. Kajzar, F.; Messier, J. Third-harmonic generation in liquids. *Phys. Rev. A* **1985**, *32*, 2352–2363. [[CrossRef](#)]
140. Débarre, D.; Beaufrepaire, E. Quantitative characterization of biological liquids for third-harmonic generation microscopy. *Biophys. J.* **2007**, *92*, 603–612. [[CrossRef](#)]
141. Novelli, F.; Tollerud, J.O.; Prabhakaran, D.; Davis, J.A. Persistent coherence of quantum superpositions in an optimally doped cuprate revealed by 2D spectroscopy. *Sci. Adv.* **2020**, *6*, eaaw9932. [[CrossRef](#)]



© 2020 by the authors. Licensee MDPI, Basel, Switzerland. This article is an open access article distributed under the terms and conditions of the Creative Commons Attribution (CC BY) license (<http://creativecommons.org/licenses/by/4.0/>).